JOURNAL OF SYNCHROTRON RADIATION

ISSN 1600-5775

Influence of diffuser grain size on the speckle tracking technique

Naxi Tian,[a,b,c] Hui Jiang,[a,b]* Aiguo Li,[a,b]* Dongxu Liang,[b] Shuai Yan[b] and Zengyan Zhang[a,b]

[a]Shanghai Institute of Applied Physics, Chinese Academy of Sciences, Jiading District, Shanghai 201800, People's Republic of China, [b]Shanghai Synchrotron Radiation Facility, Shanghai Advanced Research Institute, Chinese Academy of Sciences, Zhangheng Road 239, Pudong District, Shanghai 201204, People's Republic of China, and [c]University of Chinese Academy of Sciences, Beijing 100049, People's Republic of China. *Correspondence e-mail: jianghui@sinap.ac.cn, aiguo.li@sinap.ac.cn

Received 8 June 2019
Accepted 11 November 2019

Edited by P. A. Pianetta, SLAC National Accelerator Laboratory, USA

Keywords: speckle; phase contrast; dark field; grain size; resolution.

The speckle-based X-ray imaging technique (SBT), which includes the three imaging modalities of absorption, phase contrast and dark field, is widely used in many fields. However, the influence of the grain size of the diffuser, the coherence of the X-ray source and the pixel size of the detector on the multi-mode imaging quality of SBT is still woefully unclear. In this paper, the whole SBT process is simulated and the influence of these three factors on image quality is discussed. Based on this discussion, the grain size of the diffuser for SBT applications should be limited by the pixel size of the detector and the coherence length of the X-ray source. According to analysis of the noise signal and correlation map, a suitable grain size is an indispensable condition for high-quality SBT images, because an excessively small or large grain size degrades the resolution of the imaging results and generates false signals. In addition, the power spectral density of the measured raw speckle patterns demonstrates that a smaller grain can better retain high-frequency information from an imaged sample. The simulated and experimental results verify these conclusions. The conclusions of this work will be helpful in designing suitable experimental setups for SBT applications and have the potential to promote the performance of SBT in other applications, such as X-ray optics metrology and coherence measurement.

1. Introduction

Recently, X-ray imaging techniques have been vastly improved by the high brilliance and high penetration depth of synchrotron radiation. As the most direct and traditional X-ray imaging modality, absorption imaging can provide basic absorbing contrast information from samples. In order to further analyze detailed features of samples, the subsequently developed phase-contrast (Momose, 2005) and dark-field imaging techniques (Pfeiffer *et al.*, 2008) can also be used. With its higher sensitivity to small density deviations, phase-contrast imaging can obtain superior results from samples that have weak absorption structures, such as the soft tissues of biological samples. Dark-field imaging allows the collection of scattering information about samples. It has satisfactory abilities to display the scattering structure of samples.

Several methods have been developed to achieve these multiple advanced imaging schemes, including propagation-based (Weitkamp *et al.*, 2011), grating-based (Pfeiffer *et al.*, 2006) and speckle-based methods (Berujon *et al.*, 2012*a*). The propagation-based method is effective in determining the high-frequency information from samples but this method is insensitive to slowly varying phase gradients. Except for its

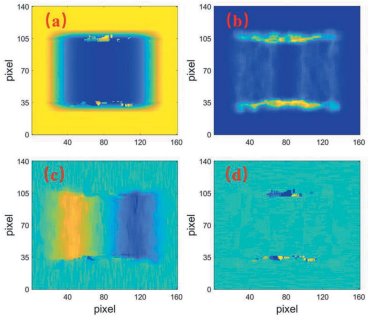

application in imaging, the grating-based technique (GBT) is useful for the metrology of reflective optics (Berujon & Ziegler, 2012) and the optimization of bimorph mirrors (Wang *et al.*, 2014). The key optical components of GBT are gratings, and imaging with this technique usually requires at least two gratings in its setup. Additionally, the optical configuration of GBT is complex, and the cost of gratings is expensive. Compared with GBT, the speckle-based technique (SBT) replaces the grating pattern with a speckle pattern that is generated from the scattering of random-phase objects (the diffuser). SBT simplifies the setup of experiments and the diffusers are generally biological membranes or sandpapers, which are much cheaper than gratings. In addition, SBT has a higher contrast-to-noise ratio than GBT in phase-contrast imaging (Romell *et al.*, 2017) and can avoid the phase unwrapping problem (Kashyap *et al.*, 2016*a*). With these unique properties, SBT has been applied in various fields, such as testing the performance of Kirkpatrick–Baez (K-B) focusing systems (Kashyap *et al.*, 2016*b*), the measurement of the transverse coherence of a synchrotron radiation source (Kashyap *et al.*, 2015) and the optimization of bimorph X-ray mirrors (Wang *et al.*, 2015).

The basic principle of SBT relates to the scattering properties of near-field speckles (Berujon *et al.*, 2012*b*). In the near-field region (Fresnel diffraction region), the size and shape of speckles remains unchanged. This property allows speckles to be employed as wavefront modulation markers instead of gratings. As a result of this property, it is easy to reconstruct the special features present in samples by recording two speckle patterns generated from a diffuser at the same position. One speckle pattern, termed the 'reference image', only contains the information of the diffuser, while the other speckle pattern, called the 'sample image', contains information from both the diffuser and the sample. Because the near-field speckle is unchanged, the displacement introduced by a sample can be contained in the sample image. This displacement caused by samples is related to the change of the wavefront gradient, which is the derivative of the phase information from the sample (Berujon *et al.*, 2012*a*). The digital image correlation (DIC) algorithm is used to calculate this displacement with subpixel accuracy (Pan *et al.*, 2009).

Although SBT has been implemented and tested in many fields (Kashyap *et al.*, 2016*b*), the factors influencing the imaging results still need to be investigated. As the key point of SBT, the speckle patterns acquired by the detector are mainly determined by four elements (Berujon *et al.*, 2012*b*): the size feature of the diffuser, the coherence of the incident source, the response function of the detector and the Talbot effect. The entire loss of certain frequencies caused by the Talbot effect can be avoided by using a source with sufficiently large bandwidth (Berujon *et al.*, 2014). However, there is still a lack of studies on the influence of the other three elements. In a previous study, it was mentioned that adjusting the grain size of the diffuser to match the detector resolution could increase the contrast of the interference fringe (Berujon *et al.*, 2014). However, it was determined that an increased grain size of the diffuser cannot effectively change the root-mean-square (RMS) error of the calculated phase-contrast results (Aloisio *et al.*, 2015). In addition, it was also mentioned that a smaller average size of speckles could improve the intensity of dark-field signals (Wang *et al.*, 2016). However, the practical influence of the grain size on SBT for achieving the desired imaging quality is still unknown. SBT requires a moderate coherence in both imaging (Kashyap *et al.*, 2016*a*) and metrology (Wang *et al.*, 2015). In previous studies, the influence of coherence was mainly on determining a suitable experimental distance (Berujon *et al.*, 2014). The influence of the detector has also been mentioned in some works. In particular, the response function of the detector has been shown to degrade the quality of speckle patterns (Berujon *et al.*, 2014), and SBT can be successfully performed even with a low exposure time of 0.5 ms (Aloisio *et al.*, 2015). However, comprehensive studies discussing the relationship between the grain size, coherence and detector pixel are still lacking.

In this paper, based on a discussion about the generation process of the speckle patterns for SBT, we dissect the influence of the diffuser grain size, the detector pixel size and the partial coherence of the synchrotron radiation source on SBT imaging. We propose a practical method to give a suitable grain size range of the diffuser for SBT. We then simulate the whole SBT process with a diffuser with diverse grain sizes to verify our discussion and grain selection method. Measured SBT results using a gold mesh confirmed our simulations. In addition, both our simulated and experimental results showed that a smaller grain size can ensure a higher imaging resolution for SBT. Through our discussion about noise analysis and the correlation map of a single point, we explain the above-mentioned features of smaller grain size in SBT and analyze the formation process of false signals appearing in the imaging results. Moreover, we discuss the frequency feature of different grain sizes using power spectral density results.

2. Theory and simulation

A speckle is the summation of mass random independently phased additive complex components that has random amplitudes and phases (Goodman, 2006). Generally, it arises from the diffuse reflection of a rough surface. However, the generation of a speckle in the X-ray near-field region is caused by the superposition of interference fringes (Cerbino *et al.*, 2008). In the near-field region, the coherent patches of the partially coherent source have random amplitudes and phases. When one point of the diffuser is illuminated by one coherent patch, a circular fringe interference pattern is generated, caused by interference between the scattered wave of this point and the transmitted wave. Based on this model, a speckle pattern can be regarded as the superposition of many interference fringes originating from the scattering of many points of a diffuser.

Considering the generative process of near-field speckles, the intensity distribution of near-field speckle patterns can be appropriately expressed using the mutual coherence function (Kohn *et al.*, 2001),

$$I(x', z') = \iiiint \left[\left(T(x_1, z_1)\, T^*(x_2, z_2)\, \mu(x_1 - x_2, z_1 - z_2) \times \exp\left[ik(s_1 - s_2)\right]\right) \Big/ \left(\lambda^2 L^2\right)\right] \mathrm{d}x_1\, \mathrm{d}z_1\, \mathrm{d}x_2\, \mathrm{d}z_2, \quad (1)$$

where (x_1, z_1) and (x', z') represent points on the sample and detector planes, respectively, (x_2, z_2) is another point on the sample plane, L is the distance from the sample to the detector along the propagation direction z, and λ is the wavelength of the incident light. $k = 2\pi/\lambda$ is the wavenumber and $s_{1,2}$ is the distance from (x_1, z_1) and (x_2, z_2) to (x', z'), respectively. The most important two terms of this equation are the transmission function $T(x, z)$ of the sample and the spectral degree of coherence $\mu(x, z)$ of the source.

To further explain the transmission function, a diffuser can be treated as a sample that has many grains on its plane. Each grain of the diffuser is a hemisphere with radius r_i. Thus, the transmission function of the diffuser can be written as (Kohn *et al.*, 2001)

$$T(x, z) = \exp\left\{-\frac{4\pi}{\lambda}\, n \sum_{i=1}^{N} \left[r_i^2 - (x - x_i)^2 - (z - z_i)^2\right]^{1/2}\right\}, \quad (2)$$

where (x, z) is a coordinate on the diffuser plane and x_i, z_i is the center of each hemisphere. If x, z is larger than r_i for the ith grain, the value of $T(x, z)$ is zero. The different grains on the diffuser plane can be allowed to overlap with each other. The symbol $n = 1 - \delta + i\beta$ represents the complex refractive index of the sample; δ and β are the refractive and absorption indices, respectively. This equation indicates that the influence of a diffuser on the generation of a speckle pattern is related to its grain size r. A similar opinion has been given by Kohn *et al.* (2001), who stated that the size of speckles generated from the diffuser in the near-field region relates to the feature of the diffuser grain. Moreover, after introducing a sample into the transmission function, the total transmission function in equation (1) will be changed to $T(x, z)\, T_s(x, z)$. This replacement indicates that the sample is modulated by the speckles of the diffuser.

With regard to the coherence, the emitted light from a synchrotron radiation source is partially coherent light and can be expressed by the Gaussian Schell model. For a partially coherent source, its spectral degree of coherence can be written as (Wang *et al.*, 2011)

$$\mu(x, z) = \exp\left\{-\left[\frac{(x_1 - x_2)^2}{2l_x^2} + \frac{(z_1 - z_2)^2}{2l_z^2}\right]\right\}, \quad (3)$$

where l_x and l_z are the coherence lengths of the source in the horizontal and vertical directions, respectively. l_x and l_z are related to the size of the source and the propagation distance from the source (Kohn *et al.*, 2001). A smaller source size or a larger propagation distance can yield a higher value of $\mu(x, z)$. This equation reflects the influence of coherence. On the one hand, if the coherence length $l_{x,z}$ is larger than r, the correlation of any two points of each grain is high enough to generate phase-based speckles (Wang *et al.*, 2016). This kind of speckle has features of the near-field speckle and can be used as a wavefront modulator in SBT. However, if $l_{x,z}$ is smaller than r, the value of $\mu(x, z)$ will drop gradually to zero and the intensity calculated by equation (1) is just the absorption contrast of the diffuser. This absorption-based speckle will lose certain information about a sample. Moreover, the insufficient coherence length of the source can decrease the visibility of speckle patterns (Kohn *et al.*, 2001). On the other hand, the experiment distance is determined by the coherence length. In the far-field region, the diffraction integral will transform to Fraunhofer diffraction (Sikorski *et al.*, 2015) and the speckle will be enlarged in the propagation direction (Cerbino *et al.*, 2008).

Besides grain size and coherence, the sampling limit of the detector is also important. In reality, the intensity is recorded by the detector and sampled according to the pixel size of the detector. Because the width of the source is generally different in the horizontal and vertical direction, the detector pixel size refers to the width of a single pixel and represents the sampling effect of the detector in the two directions.

The quality of the speckle patterns critically determines the performance of the DIC algorithm (Momose, 2005). Considering the above-mentioned three influencing factors, the near-field speckles should have the size of the diffuser grain size. However, the coherence length of the source and the pixel size of the detector limit the optional range of the grain size. Therefore, the appropriate grain size of the diffuser for SBT should be large enough to satisfy the sampling limit of the detector and smaller than the coherence length at the diffuser position. This limitation ensures that the speckles generated in SBT are near-field speckles. Near-field speckles ensure the successful application of SBT.

Based on these theoretical discussions, we simulated the whole imaging process of SBT with different grains in a diffuser to verify our discussion. To simplify the simulation and ensure the coherence length was sufficient for all grains, the incident beam was assumed to be collimated (the magnification was 1) and fully coherent. Our calculations were based on the near-field Fresnel approximation of the diffraction integral (Zdora *et al.*, 2015). The transmission function of the diffuser and the simulated sample could be acquired based on the thickness distributions and the complex refraction index of the diffuser and sample, respectively. The diffuser was simulated as sandpaper made of SiC, and the sample material was Au. To approach a true grain distribution for the sandpaper, the radius distribution and the position distribution of each hemisphere located on the sandpaper all corresponded to a Gaussian distribution with a standard deviation of 20%, and the sample was specially designed with a slow-varying triangular phase gradient in the horizontal direction but two high-frequency jumping signals in the vertical direction. Both the thickness distribution of the sandpaper and the sample are shown in Figs. 1(*a*) and 1(*b*). The energy of the incident beam was 17 keV. The simulated speckle patterns, which are shown in Figs. 1(*c*) and 1(*d*), were calculated with a fast Fourier transform. The pixel size of the simulated detector was 0.2 µm. The multiple imaging results shown in Fig. 2 were calculated

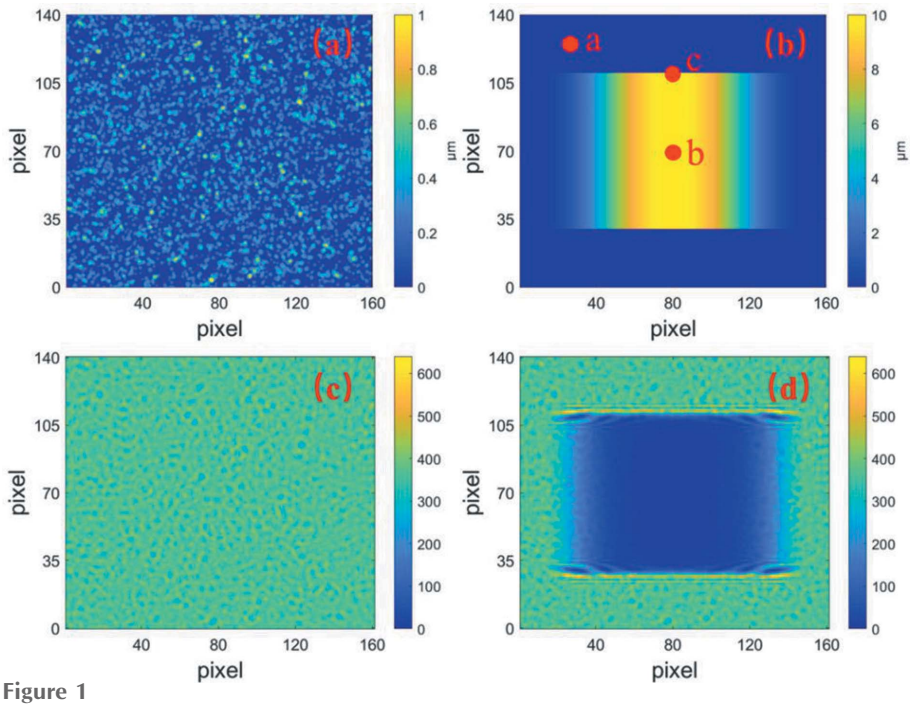

Figure 1
(*a*) Simulated sandpaper profile and (*b*) sample thickness distribution. (*c*) Simulated original speckle images of the reference image and (*d*) sample image. The diffuser grain size was 0.5 μm. The three points marked *a*, *b* and *c* in (*b*) were the external, internal and edge reference, respectively.

with a subset of 11 × 11 pixels and the searching area was 20 × 20 pixels. Since the aim of this work was to understand the influence of grains, we used the same subset in the calculation for different grains to control the variable in our comparisons. The influence of various subsets will be presented elsewhere.

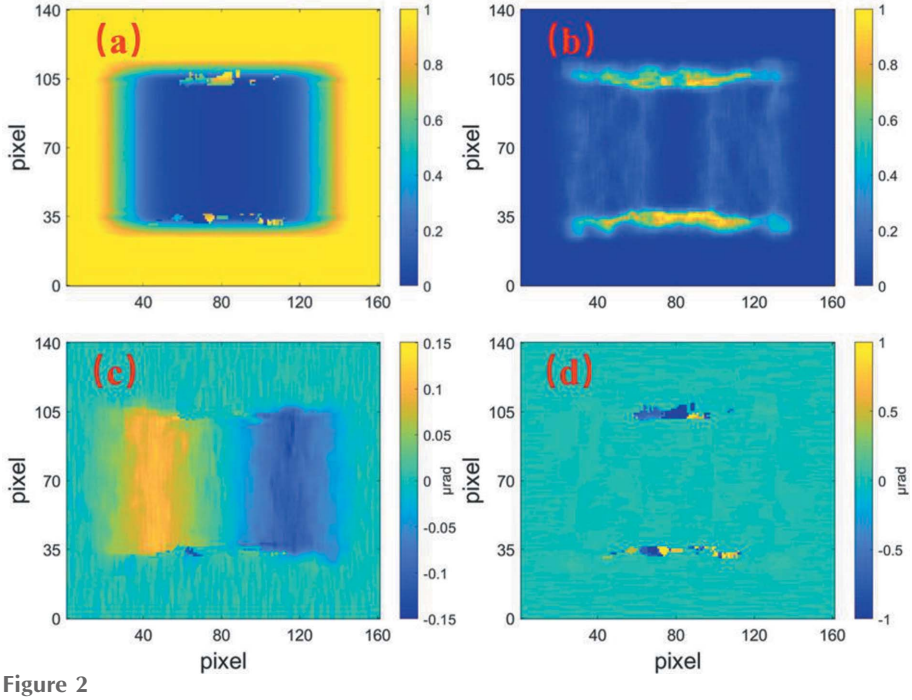

Figure 2
Multi-model imaging results, including (*a*) absorption, (*b*) dark field, (*c*) horizontal gradient and (*d*) vertical gradient phase contrasts, calculated by the DIC algorithm with a diffuser grain size of 0.5 μm.

Multiple imaging results based on simulations are shown in Fig. 2. The edge-enhancement effect was handled by the method mentioned by other researchers (Wang *et al.*, 2017). The absorption image shows the fundamental absorption information of the sample, mainly due to its thickness and absorption coefficient. In the vertical direction of the absorption image, some blurring appears at the margin of the sample [Fig. 2(*a*)]. The reason for this blurring is that SBT is insensitive to the high-frequency information of the sample, especially for such extreme phase jumping in the vertical direction. The two-phase jumpings at the vertical margins of the sample were specially designed to capture high-frequency information in our simulation. However, strong dark-field signal appeared at the two margins indicating edge scattering of the sample [Fig. 2(*b*)]. The dark-field image supplemented the scattering information of the sample, which was inaccessible in the absorption image. In addition, the phase image results corresponded to our designed phase gradient in both directions. These results clearly show a triangular phase variation in the horizontal direction and two-phase jumpings in the vertical direction.

To compare the influence of different grains, the one-dimensional phase gradient calculated from different grains is shown in Fig. 3. In the horizontal direction, the slow-varying phase gradient is clear in Fig. 3(*a*). In the vertical direction, the phase jumping makes it difficult to calculate an accurate true value. However, the position of the sample edge can be determined by the vertical phase gradient result. In Figs. 3(*a*) and 3(*c*), a grain size of 0.5 μm yields the most precise phase gradient in the horizontal direction and the most precise edge position in the vertical direction. Compared with the theoretical phase gradient, a smaller or a larger grain leads to a horizontal phase gradient with higher noise and a vertical edge sharp peak with a larger extension or a larger position error. In addition, in Figs. 3(*b*) and 3(*d*), comparing the theoretical phase gradient, a grain size of 0.5 μm had the smallest RMS value and a smaller displacement error than the other grains. Moreover, the RMS value, the displacement error and the

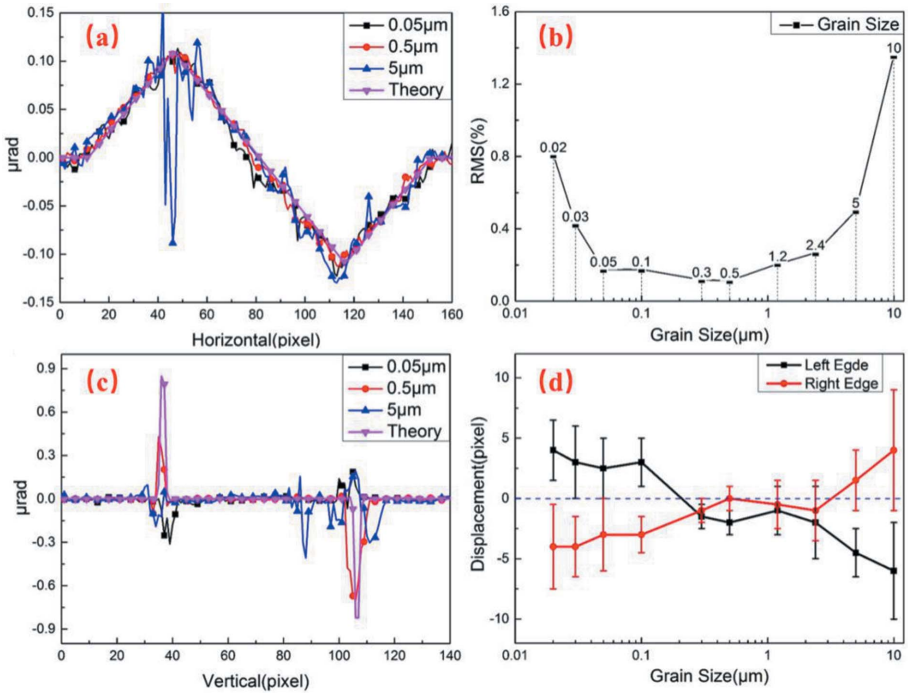

Figure 3
(*a*), (*c*) One-dimensional phase gradient compared with theoretical values in the horizontal and vertical direction. (*b*) RMS results of the phase gradient acquired by changing the grains of the diffuser. (*d*) Edge displacement error acquired by different grains compared with the theoretical position; the length of the error bars is the width of the calculated edge. The direction of the displacement error on the left-hand side of the edge is negative and on the right-hand side is positive.

width of the edge peak increased when the grain size was smaller than the sampling limit of the detector (the pixel size was 0.2 μm) or close to the thickness of the sample (10 μm). These results showed that a grain size of 0.5 μm, which is close to the limit of the detector pixel width, was the optimal grain size under the selected range from 0.02 μm to 10 μm. The other thing that needs to be focused on in Fig. 3(*d*) is that the calculated width of the sample in the vertical direction increased with grain size increase, since the displacement error direction changed outside the sample.

To simulate the real experimental situation and further analyze the difference between various grains, we added a Gaussian noise with different signal-to-noise ratio (SNR) value in our simulation to study the anti-noise capability of different grains.

As is shown in Fig. 4(*a*), the smaller grain (0.05 μm) gave the poorest anti-noise performance. Even though the noise level was low (SNR = 20 dB), the completely incorrect phase gradient result was calculated. The middle-sized grain (0.5 μm) gave the best anti-noise performance. When the SNR was larger than 10 dB, the phase gradient for the middle-sized grain was calculated with few errors. The larger grain (5 μm) just resisted low-level noise. Its anti-noise capability was weaker than the middle-sized grain. These noise results show that a smaller grain (which satisfies the limit of the detector pixel size) also has stronger anti-noise capabilities.

The reasons for the different performance of the various grains in SBT can be analyzed using the results from the correlation maps shown in Fig. 5. The DIC algorithm is used to calculate the imaging result in SBT and a high calculation precision in DIC always means a high imaging resolution in SBT. In the DIC algorithm, the displacements introduced by the sample are calculated using the position of the maximum cross-correlation peak (Pan *et al.*, 2009). Here, the speckles generated by the diffuser were the markers in the DIC calculation. Therefore, the grains that are selected in the subset are used to calculate the correlation map in the searching area of the sample image (Pan *et al.*, 2009). The correlation map then records the correlation coefficient between two subsets that are selected from the reference image and sample image at each pixel in the searching range. The searching area was a rectangular area that consisted of neighboring pixels close to the central pixel of the subset. For each subset in the reference image, one absolute maximum correlation peak and some satellite peaks (local maximums) appear in the correlation map, and the distance of the adjacent peaks relates to the grain size of the diffuser. The displacement of the maximum correlation peak is caused by the sample. However, under two conditions, many peaks existed in the correlation map that had similar values to the absolute maximum correlation peak caused by the sample. The first condition was that the change of the local feature around the sample was stronger than the feature of grain. The second condition was that the subset contained insufficient information about the sample since the selected markers (speckles) were insufficient in this subset. These similar peaks prevent the DIC algorithm from finding the precise absolute maximum correlation peak and generate a false signal.

Comparing Figs. 5(*a*.1), 5(*b*.2) and 5(*c*.3), the correlation coefficient was found to be different at different positions of the sample. In the pure sandpaper area [Figs. 5(*a*.1), 5(*a*.2) and 5(*a*.3)], one strong sharp peak appears compared with the other satellite peaks and the full width at half-maximum (FWHM) of this maximum correlation peak increases as the grain size increases. This means that smaller grain sizes lead to higher resolution in DIC, since a sharp peak can ensure a more precise displacement calculation. At the inner point of the slow-varying region of the sample [Figs. 5(*b*.1), 5(*b*.2) and 5(*b*.3)], although the correlation coefficient of the satellite peaks increased, the value of the maximum correlation peak was still much larger than for the satellite peaks, and the DIC algorithm calculated the correct displacement for all three grains. However, at the sample margin, the smallest grain size of 0.05 μm led to an incorrect displacement in both directions

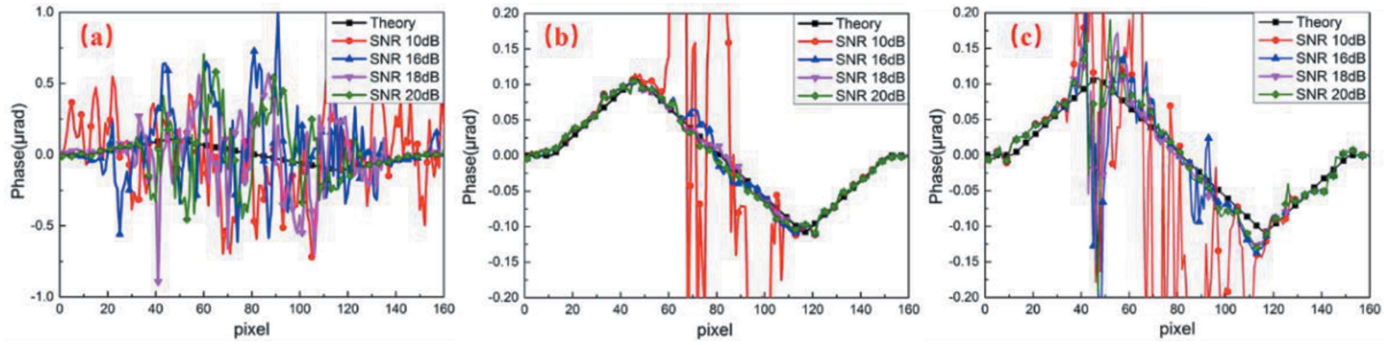

Figure 4
Horizontal phase gradient (with different noise levels) calculated using a grain size of 0.05 μm (*a*), 0.5 μm (*b*) and 5 μm (*c*).

with a value of zero [Fig. 5(*c*.1)]. This is because the grain size of 0.05 μm exceeded the sampling restriction of the detector. When the grain size is less than the sampling limit of the detector, the speckle pattern recorded by the detector contains the incorrect sample information and the signal contains more noise. Therefore, a grain size that is smaller than the limit of the detector yields a low imaging resolution and has a poorer anti-noise capability. In addition, larger grains can also have an incorrect displacement. One reason for this is that larger grains lead to a wider maximum correlation peak in the correlation map which means a decreased discernibility ability of the larger grains. Another reason is that the marker in the constant subset is only one grain since the subset size was 2.2 μm. The decreased grain markers in the subset reduce the visibility of the speckles, and characteristic information about the sample is missed. Therefore, larger grains lead to an incorrect maximum correlation peak in the correlation map and generate false signals [Fig. 5(*c*.3)]. The

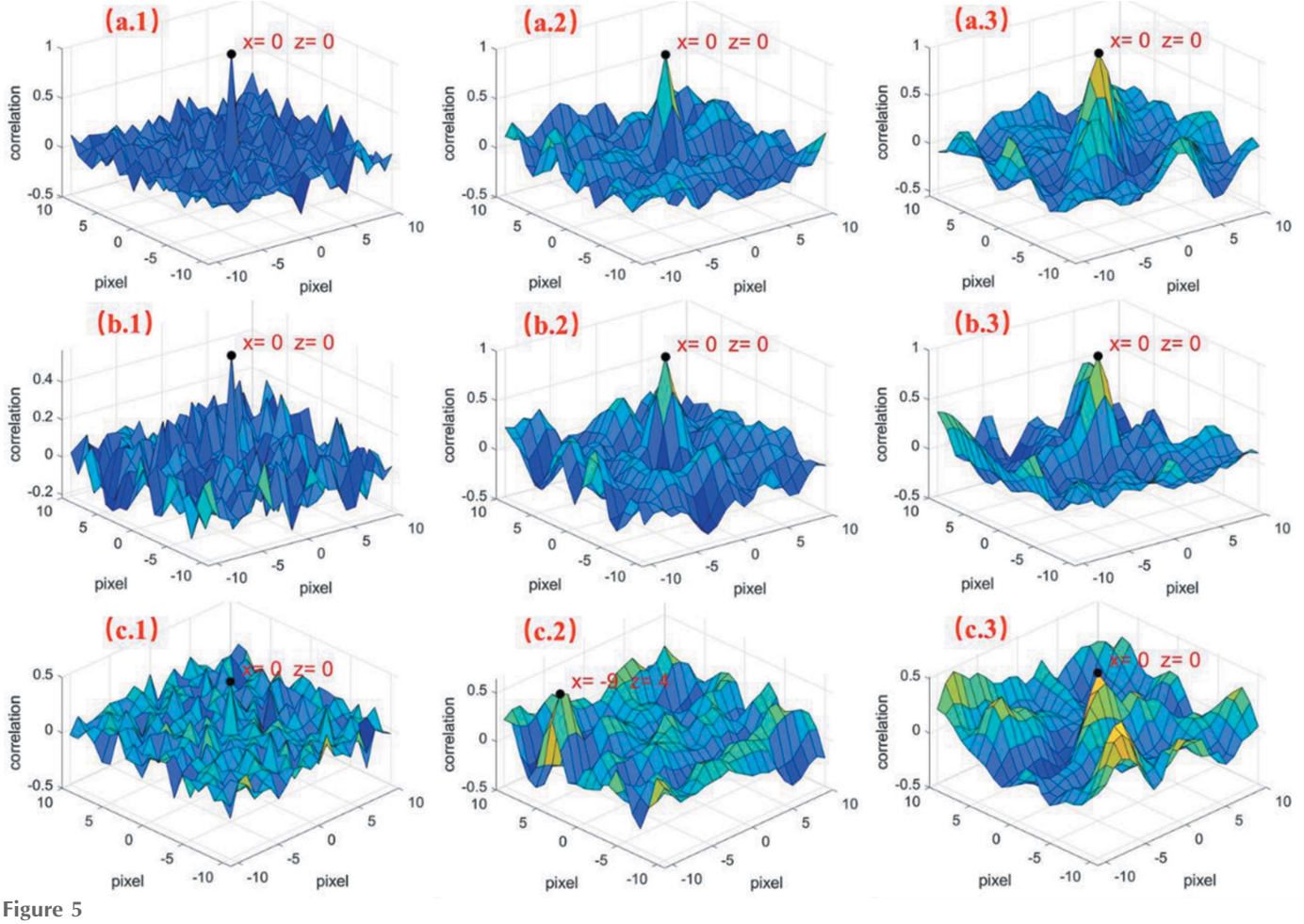

Figure 5
Correlation maps of a single point calculated in the search range for grain sizes of 0.05 μm (denoted by 1), 0.5 μm (denoted by 2) and 2.4 μm (denoted by 3). (*a*) Outside the sample, (*b*) inside the sample and (*c*) at the sample margin. These three points are denoted in Fig. 1(*b*).

decrease of the anti-noise capability for larger grains was due to these two reasons, also. As shown in Fig. 5(*c*.2), a grain size of 0.5 µm leads to the correct displacement at the sample margin and has lower satellite peaks in the correlation map. This is because a grain size of 0.5 µm is the smallest grain size that satisfies the sampling requirement of the detector and ensures sufficient speckle grain markers for the selected subset. This also means that a grain size of 0.5 µm has a stronger anti-noise capability when the subset is constant.

These correlation map results for a single point validate the limit effect of the detector in the appropriate optional grain size range for SBT. They also demonstrate that a smaller grain size that satisfies our method can ensure higher imaging resolution, fewer false signals and better anti-noise capability in DIC. Therefore, to gain a higher imaging resolution for SBT, our advice is to choose a grain size of the diffuser close to the detector limit using the grain select method discussed previously.

3. Experiment

To demonstrate the above-mentioned method in this work, a series of SBT experiments were performed using the hard X-ray micro-focusing beamline (BL15U1) of the Shanghai Synchrotron Radiation Facility (SSRF) (Wang *et al.*, 2011; Momose, 2005). The experimental scheme is shown in Fig. 6. The working energy was adjusted to E = 17 keV (λ = 0.073 nm) with a Si (111) monochromator ($\Delta E/E = 10^{-4}$). The size of the incident beam was sheared by a slit. After that, the incident beam was focused by a subsequent K-B focusing system.

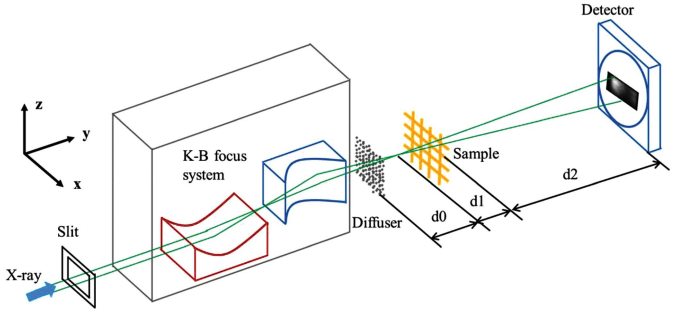

Figure 6
Basic scheme of an SBT experiment. After being focused by the K-B system, an X-ray beam illuminates the sandpaper to generate speckles, which are adjusted by the sample and ultimately gathered by the detector.

Table 1
Detailed parameters of the sandpaper used in this work.

Grit designation	Average grain size (µm)	Brand and texture
800	~10	MATADOR
2500	~5	
5000	~2.4	Wasserfest (SiC)
7000	~1.2	
12000	~0.5	3M (Mylar)
18000	~0.3	

Sandpaper was installed at a defocus position at a distance d_0 = 71 mm upstream of the focus. In order to verify the influence of the diffuser on SBT, we chose six different grains of sandpaper in this experiment (see Table 1).

A gold mesh was then placed behind the focus at a distance d_1 = 0.8 mm and the effective detection region of the mesh was one of its crosshairs with a diameter of 10 µm [Fig. 7(*b*)].

The speckle patterns [Fig. 7(*c*)] were collected by a detector (Photonics Science) with a pixel size of 13 µm × 13 µm, which was installed downstream of the sample at a distance d_2 = 1639.2 mm. However, considering the magnification of the experiment, the effective pixel size at the sandpaper location was approximately 0.15 µm in the horizontal direction and 0.18 µm in the vertical direction. Additionally, each exposure time was set to 5 ms, and each final speckle pattern was the average of five exposures in order to decrease the random noise of the detector.

4. Result and discussion

Multi-modal X-ray imaging results of the crosshair [shown in Fig. 7(*b*)] calculated using different grains are shown in Fig. 8. The absorption image [Fig. 8(*a*.1)] provides substantial contrast of the crosshair. In Fig. 8(*a*.1), an arcuate corner is shown in the left part of the crosshair (red rectangle region) since the corner of the crosshair was not a perfect right-angle. An increased dark-field signal appears in the same region of the dark-field image [Fig. 8(*b*)1] demonstrating this conclusion again. In addition, this feature of the corner can be observed in the same region of two differential phase gradient images

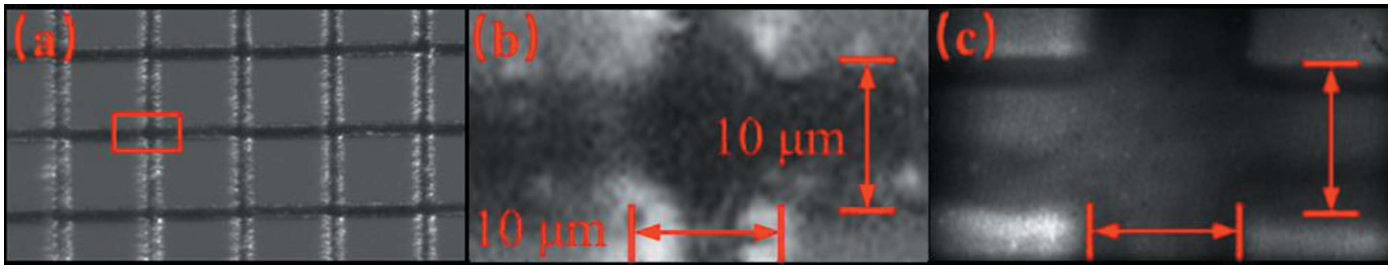

Figure 7
(*a*) Original image of the mesh acquired by microscopy. (*b*) One local part of the mesh, highlighted in the red rectangle in (*a*), is a crosshair with a symmetrical structure. The bright margins of the crosshair are caused by the lighting source of the microscope. (*c*) The corresponding speckle image of the cross hair; the crosshair is shown in (*b*).

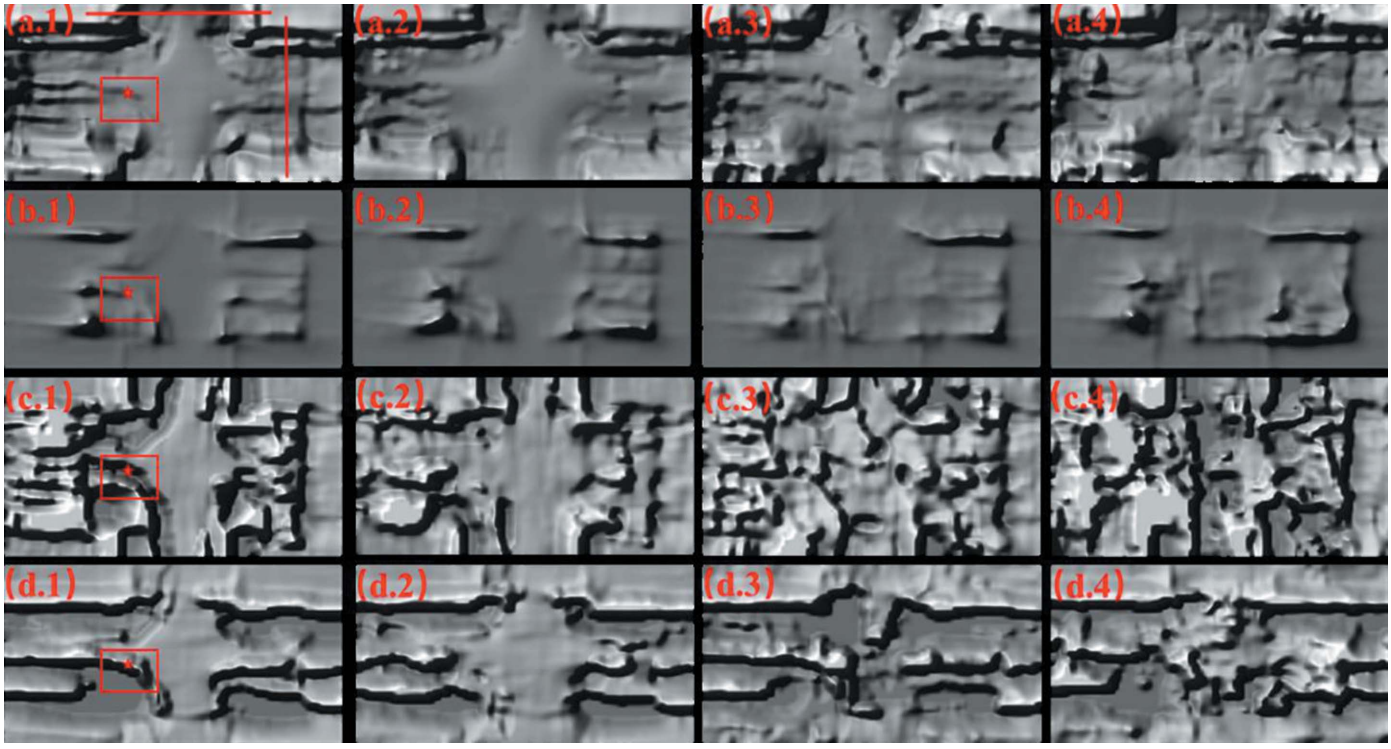

Figure 8
Multi-modal X-ray imaging results calculated using a grain size of 0.3 µm (denoted by subscript 1), 1.2 µm (denoted by subscript 2), 5 µm (denoted by subscript 3) and 10 µm (denoted by subscript 4). (*a*) Absorption, (*b*) dark-field, (*c*) horizontal differential phase gradient, and (*d*) vertical differential phase gradient. The red rectangle and the star symbol are the two positions of interest. The corresponding 1D results extracted from the position at the two red lines are shown in Fig. 9.

[Figs. 8(*c*.1) and 8(*d*.1)]. As mentioned earlier, the dark-field and phase-imaging results supplement the information of the sample that is inaccessible in an absorption image. For a local feature of the sample, through a comparison of the results of these three imaging models, a more comprehensive understanding of a sample can be obtained. In addition, in the same region, the intensity of this feature about the sample decreased with increasing grain size. Finally, this feature disappears in the results acquired using a grain size of 10 µm [Figs. 8(*a*.4), 8(*b*.4), 8(*c*.4) and 8(*d*.4)]. A similar change for another point can also be found in the one-dimensional (1D) result that is represented by dotted vertical line 4 in Fig. 9(*d*). The SNR in this experiment was about 16 dB for all grains. Based on the noise results in our simulation, smaller grains have a better anti-noise capability than larger grains at this noise level. Moreover, this feature position of the sample also exists in the dark-field and phase-gradient results [Figs. 9(*e*) and 9(*f*)]. Therefore, it can be regarded as a signal from the sample and not noise. The intensity of this feature position marked by dotted line 4 increases with decreasing grain size [Figs. 9(*e*) and 9(*f*)].

Moreover, with increasing grain size, the resolution of the arcuate corner decreased and the apparent noise signal increased in all two-dimensional (2D) results (red rectangle region). Therefore, a grain size of 0.3 µm led to the highest resolution about the crosshair, which was the smallest grain size close to the limit of the detector in our grain select method. A similar conclusion can be drawn by the 1D comparison (Fig. 9). This showed that a grain size of 0.3 µm yielded the highest precision results in the dark-field, absorption and phase results in both directions and contained the least noise interference. The 1D and 2D results of the performance of a grain size of 0.3 µm also show that smaller grains have a stronger anti-noise capability than large grains under an experiment noise level of 16 dB. The experiment results among different grains were consistent with our simulation results.

The correlation map of a single point can explain the disappearance of the arcuate corner and the degraded image quality for larger grains. The grains selected in the subset contained different information in the calculation process of creating the correlation map. Just as we analyzed in Section 2, in the area outside of the crosshair the subset contained pure sandpaper information and yielded one maximum correlation peak in the center of the correlation map. In the area inside the crosshair, the subset contained the crosshair information and led to the other different maximum correlation peak. However, at the margin of the sample, one part of the subset contained pure sandpaper information and the other part contained crosshair information. The calculation function of the correlation was unified in the DIC algorithm. Therefore, a messy contradiction appears in the calculation of DIC. This contradiction interferes with the DIC algorithm and prevents it from finding the correct displacement. The smaller grains

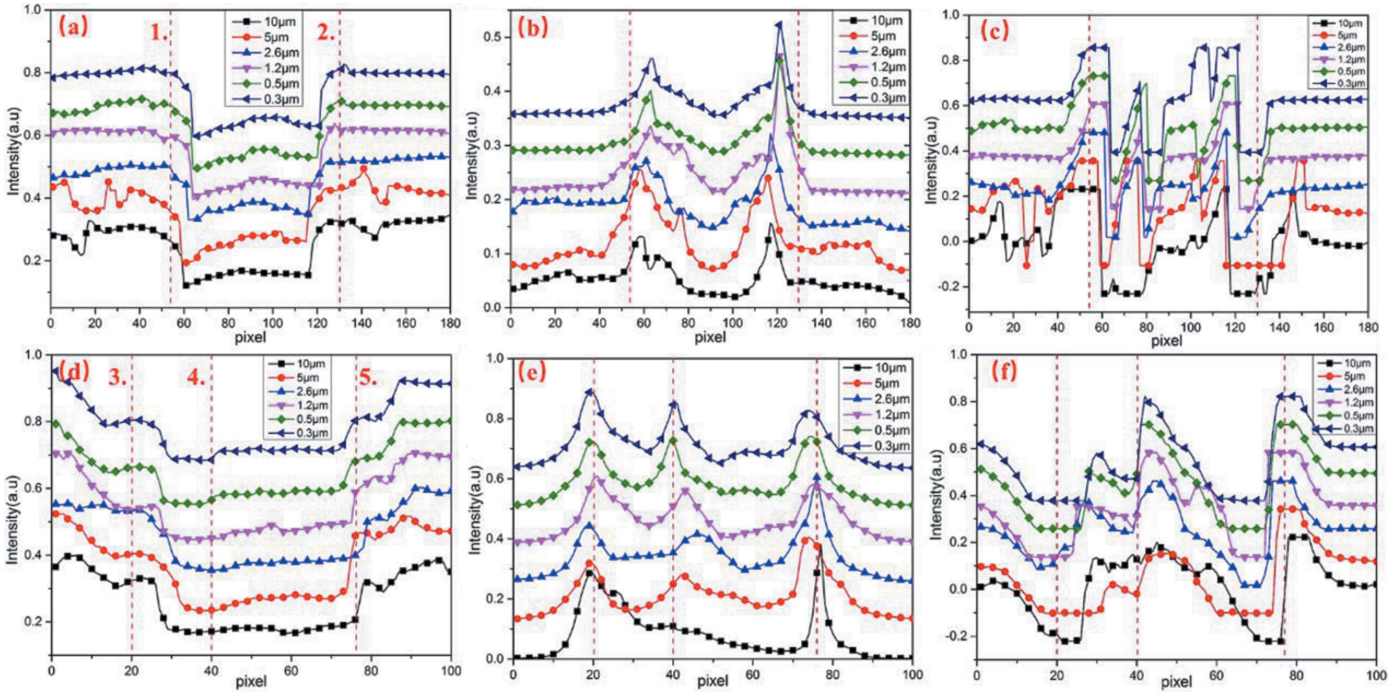

Figure 9
Comparison of 1D multi-modal imaging results among different grains. (*a*) Horizontal absorption, (*b*) horizontal dark field, (*c*) horizontal phase, (*d*) vertical absorption, (*e*) vertical dark field and (*f*) vertical phase. Dotted lines 1 and 2 are the two margins of the crosshair in the horizontal direction. Dotted lines 3 and 5 are the two margins of the crosshair in the vertical direction. Dotted line 4 is a special position of interest.

that satisfied our grain selection method can significantly avoid this situation. Therefore, a grain size of 0.5 μm leads to the correct displacement of the crosshair margin [Fig. 10(*a*)], which is similar to the simulated results in Fig. 5(*c*.2). However, because they contain less information about the sample, larger grains do not avoid the above-mentioned contradiction of the DIC. The calculated displacement was zero [Figs. 10(*b*) and 10(*c*)] and the signal of the arcuate corner disappears in the results calculated using grain sizes of 1.2 μm and 5 μm. Moreover, in Fig. 10(*d*), a grain size of 10 μm calculates an incorrect maximum correlation peak since its correlation peak has a wider FWHM. The error peaks calculated from larger grains produce false signals in the final imaging results. The experimental results of the crosshair confirmed our simulated results. This again supports the theory that a smaller grain size can yield higher resolution and lower noise signals in speckle-based multi-modal X-ray imaging.

The imaged crosshair had a symmetrical structure [Fig. 7(*b*)] and this symmetrical structure is useful for investigating the influence of partial coherence. According to the research on the luminous model of the undulator on beamline BL15U, at any distance away from the light source the ratio of the transverse coherence length and the size of the beam is constant (Wang *et al.*, 2011). Therefore, the coherence length at the sandpaper position was l_x = 0.378 μm in the horizontal direction and l_z = 4.815 μm in the vertical direction. For all of the selected grain sizes in our experiment,

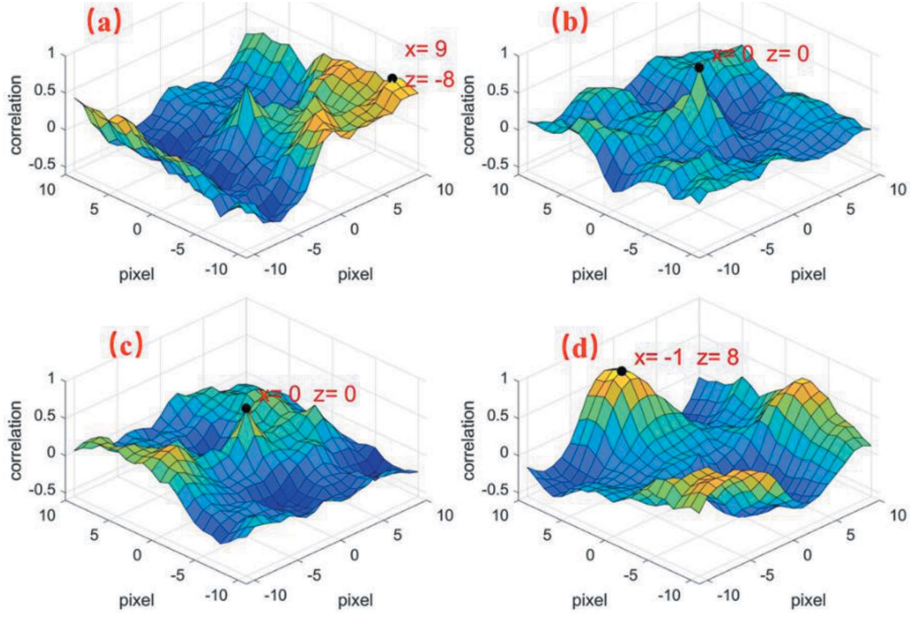

Figure 10
Correlation map of a single point calculated in the search range for grain sizes of 0.3 μm (*a*), 1.2 μm (*b*), 5 μm (*c*) and 10 μm (*d*). The point was selected at the margin of the bend and is denoted by the star symbol in Fig. 8.

a grain size of 0.3 μm satisfied the coherence limit in both directions. This was the reason why a grain size of 0.3 μm yielded the most precise 1D and 2D results in both directions. As shown by equation (3), if the grain size is larger than the coherence length, the speckles start to degrade as intensity speckles. The intensity speckles represent the absorption constant of the diffuser that misses the phase and scattering information about the sample due to the insufficient coherence. Therefore, in the horizontal direction, a grain size of 0.5 μm exceeds the coherence limit and the resolution of the 2D imaging results begins to decrease when the grain size is larger than 0.5 μm. Due to the longer coherence length in the vertical direction, the degraded imaging results begin to appear in the vertical direction when the grain size is larger than 5 μm. Also, due to the insufficient coherence length in both directions, a grain size of 10 μm led to the worst resolution compared with other grain sizes. Moreover, as a result of the insufficient coherence length in the horizontal direction, the intensity of the dark-field signal was weaker in the horizontal direction than in the vertical direction in the total 2D dark-field images [Figs. 8(*b*.1)–8(*b*.4)]. Additionally, the vertical phase results [Figs. 8(*d*.1)–8(*d*.4)] all have higher resolution and lower noise than the results in the horizontal direction [Figs. 8(*c*.1)–8(*c*.4)] and the horizontal phase results were all mixed with some vertical phase information.

The influence of coherence can also be observed in the corresponding 1D extracted multiple-model imaging results in Fig. 10. The surface of the crosshair is a curve and its absorption at the margins of the sample should have low variation. However, because of the insufficient coherence length, the absorption of the sample margins appeared in the 1D vertical absorption results [Fig. 9(*b*)] for most grains but disappeared for most grains in the horizontal absorption results [Fig. 9(*a*)]. In the dark-field results, the vertical 1D extracted dark-field results for all grains had a higher intensity than the dark-field results in the horizontal direction. Besides, the margins of the crosshair were close to the real position in all vertical 1D multiple imaging results [dotted lines 3 and 5 in Figs. 9(*d*), 9(*e*) and 9(*f*). The position of the margins was acquired from the raw speckle pattern of the crosshair and is marked in Fig. 7(*c*). However, the calculated margins of the sample all had a larger deviation in the horizontal direction [dotted lines 1 and 2 in Figs. 9(*a*), 9(*b*) and 9(*c*) as a result of the insufficient coherence length in the horizontal direction. The differences of these results between the two directions also relates to the differences of the visibility of the raw speckle patterns between the two directions. As shown by equation (3), the decreased visibility of the speckle patterns is related to the insufficient coherence length. The visibility of the speckle patterns with different grains was 0.301 ± 0.006 in the horizontal direction and 0.389 ± 0.021 in the vertical direction. A higher visibility in the vertical direction ensured a higher accuracy in the calculation of DIC (Wang *et al.*, 2016). The comparisons of 2D multi-modal imaging results between the two directions and the comparisons of the corresponding 1D extracted results between the two directions supports the influence of coherence that we discussed in Section 2. The insufficient coherence length causes the speckles to lose certain information of the sample and degrades the imaging resolution of SBT multi-model imaging.

The influence of grains and coherence on SBT can also be explained by a comparison of the power spectral density (PSD) results (Fig. 11). These PSD results were calculated using the raw speckle images of different grains (Cerbino *et al.*, 2008). Since different grains can generate speckle patterns with the features of the grains, different grains have different frequency responses in the PSD results of reference images in both directions [Figs. 11(*a*) and 11(*b*)]. In addition, since the coherence length was insufficient for almost all grains in the horizontal direction, only the low frequency of the sample was retained in the horizontal direction [Fig. 11(*c*)]. However, the vertical coherence length was sufficient for most grains. Therefore, the high-frequency information of the sample had a higher ratio in the vertical direction [Fig. 11(*d*)]. This result explains why the horizontal imaging results all had a lower imaging resolution than the results in the vertical direction, as the loss of high-frequency information about the crosshair for most grains occurred in the horizontal direction. The differ-

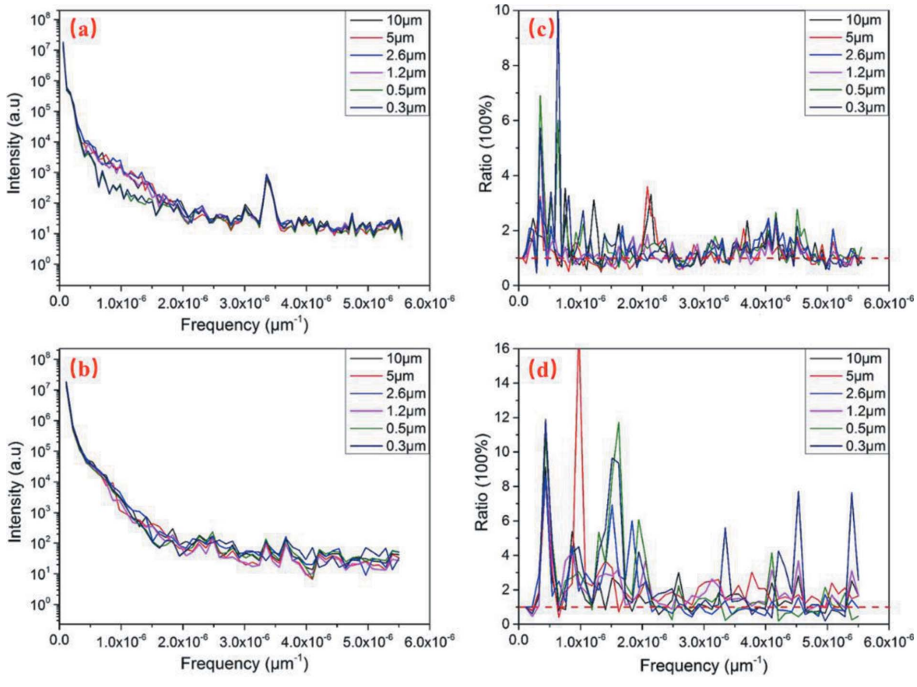

Figure 11
Comparison of PSD results for different grains. Panels (*a*) and (*b*) show the PSD results of reference images in the horizontal and vertical directions. Panels (*c*) and (*d*) show the corresponding PSD results of sample images with the reference images removed.

ence of PSD results acquired in both directions was consistent with the influence of the coherence shown from equation (3). The absorption-based speckle that was generated in the horizontal direction indeed loses some sample information. In addition, unlike the noise signal which generally covers the whole frequency domain, the four distinct signal peaks of the sample appear at the frequencies 3.4×10^{-6}, 4.2×10^{-6}, 4.5×10^{-6} and 5.5×10^{-6} μm^{-1} in the vertical direction [Fig. 11(*d*)]. The ratio of these four peaks acquired using a grain size of 0.3 μm was obviously higher than for other grains. This meant that a smaller grain can better maintain the high-frequency information of a sample, which also ensures a higher precision in the DIC calculation. These PSD results again support the influence of grains discussed in Section 2 and Section 3 and highlight the influence of coherence discussed in Section 3.

In Section 2, the comparison results of the 1D phase gradient in both directions and the correlation map of a single point for different grains were in accordance with the theoretical discussion about the influence of grains and detector pixel size. The smallest grains that satisfy the limit of the detector indeed gain higher resolution in SBT imaging. Both the 1D and 2D multi-model imaging results using different grains for the gold crosshair matched this influence of grains that we discussed and simulated. In addition, the difference between the 2D phase imaging results in the two directions matched the influence of coherence that we discussed in Section 2. The difference between the 1D extracted results from the 2D imaging results for all grains in the two directions again supported the discussed influence of coherence. The insufficient coherence length indeed caused the speckle pattern to degrade as an intensity speckle. The intensity speckle loses certain phase and scattering information of the sample. Moreover, the PSD results for all grains between the two directions show the influence of coherence and show that smaller grains can better maintain sample information than larger grains. Based on these results, the available grain size range for SBT is indeed limited by the detector pixel size and the coherence length. The smallest grain size in this available range can ensure higher imaging resolution.

5. Conclusions

The detailed influence of grain size, coherence length and detector pixel size on SBT has been discussed. The speckle patterns generated using diffusers with different grain sizes will have the respective size features of these grains. Thus, the multi-model X-ray imaging results calculated by speckle patterns will be influenced by the grain size of the diffuser. The influence of the coherence length is reflected in the generation of near-field speckles in an experiment. The influence of the detector is the sampling limit of its effective pixel size. Based on these influences, we proposed that the optimal grain size range for SBT should be limited by the detector pixel size and the coherence length of the X-ray source. Our simulated and experimental results support our discussions and validate our grain optimal range. In addition, based on our discussion about noise analysis, correlation maps and PSD results, a smaller grain size that satisfies the limit of our grain selection range can achieve imaging results with higher resolution. This is because (i) a smaller grain can better maintain the high-frequency information about a sample and has a stronger anti-noise capability; (ii) a smaller grain yields a more accurate displacement in the DIC calculations through a sharper maximum correlation peak in the correlation map; and (iii) a smaller grain can avoid the contradictions of the DIC algorithm, which appear at the margin regions of a sample. The conclusions of this work are significantly helpful for improving the resolution of multi-model X-ray imaging results and optimizing the selection of experimental parameters for SBT. In future work, we will continue to verify the performance of our grain selection method for SBT in other applications such as the coherence measurement and the metrology of X-ray optics.

Acknowledgements

The authors would like to thank our colleague Dr Guohao Du's kind help for debugging of the detector.

Funding information

The following funding is acknowledged: National Natural Science Foundation of China (grant Nos. 11775295, 11805259); Youth Innovation Promotion Association, CAS.

References

Aloisio, I. A., Paganin, D. M., Wright, C. A. & Morgan, K. S. (2015). *J. Synchrotron Rad.* **22**, 1279–1288.
Berujon, S., Wang, H., Alcock, S. & Sawhney, K. (2014). *Opt. Express*, **22**, 6438–6446.
Berujon, S., Wang, H. & Sawhney, K. (2012*a*). *Phys. Rev. A*, **86**, 063813.
Berujon, S. & Ziegler, E. (2012). *Opt. Lett.* **37**, 4464–4466.
Berujon, S., Ziegler, E., Cerbino, R. & Peverini, L. (2012*b*). *Phys. Rev. Lett.* **108**, 158102.
Cerbino, R., Peverini, L., Potenza, M. A. C., Robert, A., Bösecke, P. & Giglio, M. (2008). *Nat. Phys.* **4**, 238–243.
Goodman, J. W. (2006). *Speckle Phenomena in Optics: Theory and Applications*, 1st ed. Greenwood Village: Roberts & Company Publishers.
Kashyap, Y., Wang, H. & Sawhney, K. (2015). *Phys. Rev. A*, **92**, 033842.
Kashyap, Y., Wang, H. & Sawhney, K. (2016*a*). *Opt. Express*, **24**, 18664–18673.
Kashyap, Y., Wang, H. & Sawhney, K. (2016*b*). *Rev. Sci. Instrum.* **87**, 2562–2569.
Kohn, V., Snigireva, I. & Snigirev, A. (2001). *Opt. Commun.* **198**, 293–309.
Momose, A. (2005). *Jpn. J. Appl. Phys.* **44**, 6355–6367.
Pan, B., Qian, K., Xie, H. & Asundi, A. (2009). *Meas. Sci. Technol.* **20**, 062001.
Pfeiffer, F., Bech, M., Bunk, O., Kraft, P., Eikenberry, E. F., Brönnimann, Ch., Grünzweig, C. & David, C. (2008). *Nat. Mater.* **7**, 134–137.
Pfeiffer, F., Weitkamp, T., Bunk, O. & David, C. (2006). *Nat. Phys.* **2**, 258–261.
Romell, J., Zhou, T., Zdora, M., Sala, S., Koch, F. J., Hertz, H. M. & Burvall, A. (2017). *J. Phys. Conf. Ser.* **849**, 012035.

Sikorski, M., Song, S., Schropp, A., Seiboth, F., Feng, Y., Alonso-Mori, R., Chollet, M., Lemke, H. T., Sokaras, D., Weng, T.-C., Zhang, W., Robert, A. & Zhu, D. (2015). *J. Synchrotron Rad.* **22**, 599–605.
Wang, F., Wang, Y., Wei, G., Du, G., Xue, Y., Hu, T., Li, K., Deng, B., Xie, H. & Xiao, T. (2017). *Appl. Phys. Lett.* **111**, 174101.
Wang, H., Kashyap, Y. & Sawhney, K. (2016). *Sci. Rep.* **6**, 20476.
Wang, H., Sawhney, K., Berujon, S., Sutter, J., Alcock, S. G., Wagner, U. & Rau, C. (2014). *Opt. Lett.* **39**, 2518–2521.
Wang, H., Sutter, J. & Sawhney, K. (2015). *Opt. Express*, **23**, 1605–1614.
Wang, H., Yan, S., Yan, F., Jiang, S., Mao, C., Liang, D., Yang, K., Li, A. & Yu, X. (2011). *Acta Phys. Sin.* **61**, 175–180.
Weitkamp, T., Haas, D., Wegrzynek, D. & Rack, A. (2011). *J. Synchrotron Rad.* **18**, 617–629.
Zdora, M., Thibault, P., Pfeiffer, F. & Zanette, I. (2015). *J. Appl. Phys.* **118**, 113105.